JTTEE5 10:656-665

The Effect of Post-Treatment of a High-Velocity Oxy-Fuel Ni-Cr-Mo-Si-B Coating Part 2: Erosion-Corrosion Behavior

S. Shrestha, T. Hodgkiess, and A. Neville

(Submitted 28 July 2000)

In this paper, a study of the erosion-corrosion characteristics of a Ni-Cr-Mo-Si-B coating applied by the high-velocity oxy-fuel (HVOF) process on to an austenitic stainless steel (UNS S31603) substrate are reported. The coatings were studied in the as-sprayed condition, after vacuum sealing with polymer impregnation and after vacuum furnace fusion. The erosion-corrosion characteristics were assessed in an impinging liquid jet of 3.5% NaCl solution at 18 °C at a velocity of 17 m/s at normal incidence in two conditions: (1) free from added solids and (2) containing 800 ppm silica sand. The methodology employed electrochemical control and monitoring to facilitate the identification of the separate and interrelated erosion and corrosion contributions to the erosion-corrosion process. The rates of erosion-corrosion damage were drastically accelerated in the presence of the suspended solids. The application of cathodic protection significantly reduced the deterioration process. The study showed the effect of sealing with polymer impregnation did not significantly alter the erosion-corrosion behavior of the sprayed coating. However, there was a significant improvement in erosion-corrosion durability afforded by the postfusion process. The mechanisms by which the improved performance of vacuum-fused coatings is achieved are discussed.

Keywords cermet, erosion-corrosion, HVOF spraying, silica sand, vacuum-fusion, vacuum-sealing

1. Introduction

Erosion-corrosion is a form of material degradation that involves electrochemical corrosion and mechanical wear processes encountered in components, such as subsea pump internals, impeller wear rings, and valve plugs, which handle rapidly flowing or impinging liquid streams. Such damage is accentuated when flowing slurries are highly corrosive (*e.g.*, saline water) and especially when contaminated with solid particles, and it can cause substantial operating, breakdown, maintenance, and production costs in a wide variety of industries including offshore oil and gas,[1] mineral processing,[2] and mining. In erosion-corrosion, the total material loss is often significantly in excess of the sum of the separate pure corrosion and wear processes, thus, signifying important interactions (often termed as "synergistic" or "additive" effects) between the two components.[3–6] Moreover, the deterioration mechanism is dependent on a wide range of variables that includes properties of the (1) erodent particles (kinetic energy, flux, hardness, shape, and size), (2) target material (hardness and strain hardening coefficient), and (3) environment (salinity, temperature, and pH) as well as complex hydrodynamic effects, impact velocity, impact angle, *etc.*[7,8]

S. Shrestha and **T. Hodgkiess,** Department of Mechanical Engineering, University of Glasgow, Glasgow G12 8QQ, Scotland, United Kingdom; and **A. Neville,** Department of Mechanical and Chemical Engineering, Heriot-Watt University, Riccarton, Edinburgh EH14 4AS, Scotland, United Kingdom. Contact e-mail: suman.shrestha@twi.co.uk.

Much of the recent work investigating erosion-corrosion rates and mechanisms has been focused towards metallic materials, ranging from low-grade cast irons and carbon steels to the higher grades of austenitic and duplex stainless steels and high-grade nickel alloys.[3–5,9] Because of the vulnerability of metallic materials in aggressive erosion-corrosion conditions, there is a strong incentive for alternative surface engineering options to be developed and implemented to more efficiently resist damage by this cause.

Ceramic-base materials represent potential materials to replace metals in components for service in high wear conditions, and there has been extensive consideration of thermal-sprayed cermets as surface coatings on conventional metallic materials. Thermal-spray application techniques have been the subject of steady development, and in particular, the high-velocity oxy-fuel (HVOF) process is being widely used.[9–11] Cermet coatings applied by HVOF spraying have been developed primarily for wear resistant properties in dry and often high-temperature tribological conditions[12] and for thermal barrier applications,[13] but their potential for service in aqueous erosive conditions has also recently received attention.[14–20]

Corrosion studies have shown[21–24] that WC-CoCr coatings, and also the coating under investigation in the current work (Ni-Cr-Mo-Si-B), are rather vulnerable to corrosive attack in saline water by complex mechanisms associated with their microstructural features. This suggests that in aqueous erosion-corrosion environments corrosion may play an important role.

Recent work[25] has demonstrated the superiority of HVOF-sprayed Ni-Cr-Si-B coating in comparison with UNS S31603 stainless steel in erosive-corrosive slurries. However, the complex microstructure still proves to be a limitation in combating corrosion attack in both static and erosion-corrosion conditions. Thus, there is a strong incentive to improve the corrosion resistance of the coating. One strategy is to modify the surface of the

sprayed coating to consolidate the coating and, hence, remove internal and interconnected porosity. For example, laser remelting has been reported elsewhere.[26] In the present work, vacuum sealing by polymer impregnation and vacuum-furnace fusion techniques on one cermet coating have been investigated, and the consequent effects on corrosion and erosion-corrosion assessed. In Part 1,[28] the corrosion behavior is discussed, and the present paper reports the findings of a study of the erosion-corrosion behavior of the cermet-coating material with three different surface modifications in both solid-free impingement and slurry conditions. The comparative data found after postspray surface treatment suggests that there are benefits offered by the high-temperature vacuum-furnace fusion process for improving erosion-corrosion resistance.

2. Materials Investigated and Experimental Techniques

The material investigated in this program was a self-fluxing nickel-chromium-molybdenum-silicon-boron (Ni-Cr-Mo-Si-B) alloy coating, and this was studied in three different conditions:

- as-sprayed,
- after vacuum sealing by polymer resin impregnation (referred to as "vacuum-sealed"), and
- after a high temperature vacuum-furnace fusion process (referred to as "vacuum-fused").

The coating was commercially applied by the HVOF spraying process onto an austenitic stainless steel (UNS S31603) substrate using the Hobart Tafa JP-5000 high pressure HVOF system with liquid-kerosene fuel burning in oxygen. The vacuum-furnace fusion was conducted at the spraying plant and is described elsewhere.[27] The coating was sprayed onto disc samples (∅25 mm) of the stainless steel substrate. The specified composition of the coating is 67.5% Ni, 16% Cr, 3.5% Si, 3.5% B, 3% Mo, 3% Cu, 4% Fe, and 0.8% C (Tafa's powder 1275H). Details of the coating properties, composition, and spatial variations in composition throughout the coating are given in the accompanying paper.[28]

The erosion-corrosion behavior of all specimens was investigated in the polished condition. The polishing process comprised successive grinding on 240, 400, 800, and 1200 SiC grit papers and finally 6 μm diamond polishing.

The erosion-corrosion behavior was assessed as follows:

- weight loss tests carried out under solid-free liquid and solid-liquid impingement both at the free-corrosion potential and also under cathodic protection (CP) to suppress the corrosion component of degradation and, hence, quantify the synergism;
- potentiodynamic anodic polarization tests under conditions of solid-free liquid impingement and solid-liquid impingement to determine the kinetics of the pure electrochemical corrosion processes;
- postexperimental observations facilitated with light optical microscopy and scanning electron microscopy (SEM); and
- surface profilometry using the Surface Profiler (Taylor Hobson Talysurf, Series-2, Leicester, United Kingdom).

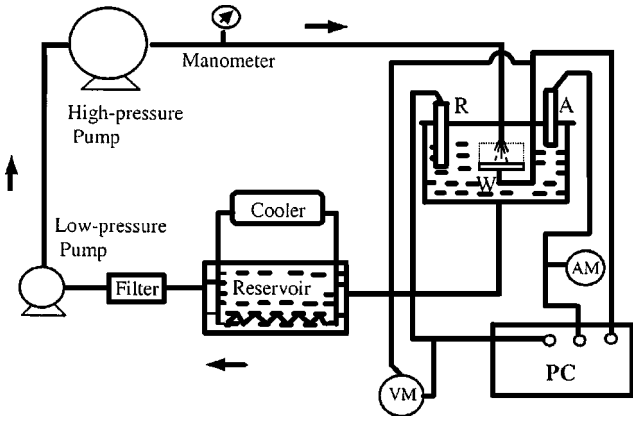

Fig. 1 Recirculating rig used for liquid impingement tests (R—reference electrode, A—auxiliary electrode, and W—working electrode)

Table 1 Particle size distribution of sand type Congleton HST60 used in solid/liquid impingement tests

Size, μm	1000	710	500	355	250	180	125	90	63
Wt.% retained	Trace	0.1	1.0	5.6	29.6	41.6	21.0	1.0	0.1

All erosion-corrosion experiments were carried out in 3.5% NaCl solution at ambient temperature, 18 to 20 °C. The solid-free impingement tests were undertaken using a circulating rig, as shown in Fig. 1, with a liquid jet of 1 mm diameter impinging at 17 m/s and 90° onto a specimen of 25 m diameter. The solid-liquid erosion-corrosion experiments used a separate but similar rig, as described in Ref 25, which also comprised a closed loop in which tests were conducted either for 1 h or multiples thereof with change of fluid hourly. The solids loading comprised 800 ppm of silica sand of almost spherical shape and a particle size distribution, as shown in Table 1. The nozzle diameter of the solid-liquid rig was 4 mm, and the impingement was again at 17 m/s and perpendicular to the specimen surface. The standoff distance for both rigs was 5 mm.

Anodic polarization scans in solid-free impingement conditions were carried out after exposure to the jet at the free-corrosion potential, E_{corr}, for 6 days. However, in the solid-liquid impingement tests, the specimens were normally subjected to 5 min impingement before starting the polarization experiment.

Samples were prepared for electrochemical tests by encapsulating them in nonconducting epoxy resin with the rear side of the specimen soldered to an electrical wire. To reinforce the isolation of the substrate material from the working fluid, nonconductive glue was applied at the specimen/resin interface. The potentiodynamic polarization tests used a standard three-electrode cell, where the potential of the working electrode (specimen) was shifted from E_{corr} to more positive potentials (at a scan rate of 15 mV/min), and the current flow in the external circuit between the sample and a platinum auxiliary electrode was measured as a function of potential. Once a current density of 500 μA/cm^2 was reached, the potential scan automatically reversed and scanned back to E_{corr}. Electrode potentials were measured using the reference saturated calomel electrode (SCE).

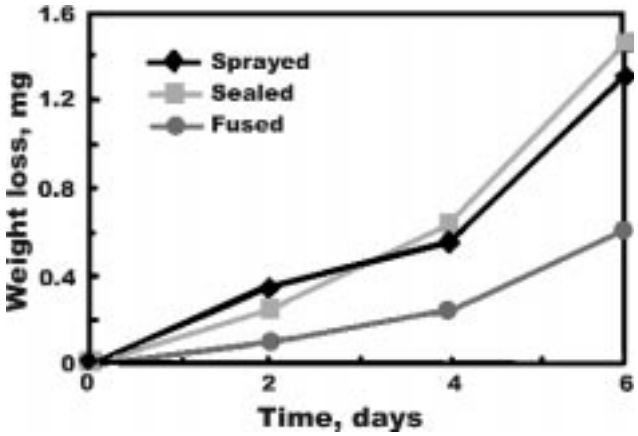

Fig. 2 Weight loss measured as a function of time for as-sprayed, vacuum-sealed, and vacuum-fused coatings (polished surfaces) in solid-free liquid impingement conditions at 17 m/s, 18 °C, and 90° impingement

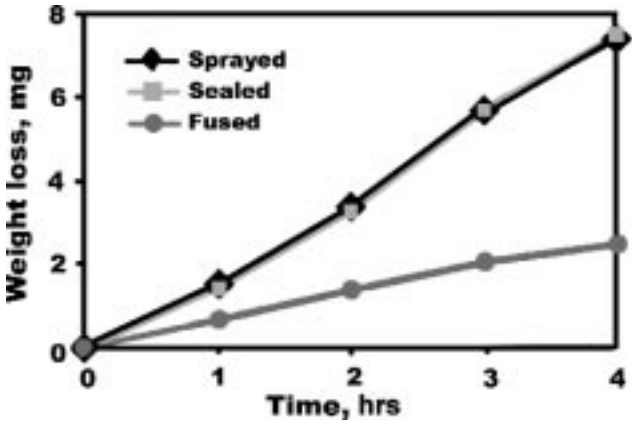

Fig. 3 Weight loss measured as a function of time for as-sprayed, vacuum-sealed, and vacuum-fused coatings in solid-liquid impingement conditions at 17 m/s, 3.5% NaCl, 800 ppm sand, and 18 °C

Table 2 Weight loss results of polished surfaces under solid-free liquid impingement at 17 m/s

Coating (polished)		TWL in milligrams under solid-free liquid impingement			Weight loss in milligrams under CP	
		2 days	4 days	6 days	2 days	6 days
As-sprayed	Sample 1	0.30	0.50	1.50	0.20	0.80
	Sample 2	0.40	0.60	1.30	0.10	0.70
	Sample 3	0.40	0.50	1.10	…	…
	Average	**0.37**	**0.53**	**1.30**	**0.15**	**0.75**
Vacuum-sealed	Sample 1	0.30	0.60	1.50	0.20	0.70
	Sample 2	0.20	0.70	1.40	0.20	0.60
	Average	**0.25**	**0.65**	**1.45**	**0.20**	**0.65**
Vacuum-fused	Sample 1	0.10	0.20	0.60	0.0	0.0
	Sample 2	0.0	0.30	0.80	0.0	0.0
	Sample 3	0.20	0.20	0.40	…	…
	Average	**0.10**	**0.23**	**0.60**	**0.0**	**0.0**

Table 3 Weight loss results of polished surfaces under solid-liquid impingement at 17 m/s

Coating (polished)		TWL in milligrams without application of CP				Weight loss in milligrams under CP	
		1 h	2 h	3 h	4 h	1 h	4 h
As-sprayed	Sample 1	1.4	3.5	5.7	7.3	0.9	3.7
	Sample 2	1.6	3.2	5.9	…	1.0	…
	Average	**1.5**	**3.35**	**5.8**	**…**	**0.95**	**…**
Vacuum-sealed	Sample 1	1.5	3.4	5.6	7.4	1.1	3.8
	Sample 2	1.3	3.1	5.7	…	0.8	…
	Average	**1.4**	**3.25**	**5.65**	**…**	**0.95**	**…**
Vacuum-fused	Sample 1	0.6	1.5	1.9	2.4	0.2	0.6
	Sample 2	0.8	1.2	2.1	…	0.3	0.6
	Sample 3	0.5	…	…	…	…	…
	Average	**0.64**	**1.35**	**2.0**	**…**	**0.25**	**0.6**

Total weight loss (TWL) was measured by weighing the specimen before and after the impingement tests to an accuracy of 0.1 mg. The liquid impingement tests under free-corrosion potential were carried out for periods of up to 6 days whereas the solid-liquid impingement tests were performed only up to 4 h. Weight loss was also measured in experiments in which the specimen was cathodically protected, by holding the potential at −0.8 V (SCE), in order to suppress corrosion. After the experiment, specimens were washed with water, and then immersed for a few seconds in an inhibited acid solution (Clarke's solution) to remove all remaining corrosion products from the surface before drying and weighing.

After the erosion-corrosion tests, the depth of the wear scar was measured using surface profiling stylus equipment. Additionally, the specimens were examined using light optical and scanning electron microscopy (SEM).

3. Results

3.1 Weight Loss Measurement

Under solid-free liquid impingement at 17 m/s, both as-sprayed and vacuum-sealed coatings (Fig. 2) exhibited similar weight loss trends during the 6-day tests with an indication of increased material loss rates occurring at longer times. The vacuum-fused coating, however, showed significantly lower weight losses compared to the as-sprayed and vacuum-sealed coatings. A smaller relative increase in weight loss between 4 and 6 days exposure was measured on the vacuum-fused coating. The average values are calculated from a range of experiments for each coating, which are shown in Tables 2 and 3. As shown in Table 2, the application of CP significantly reduced the total material losses in both as-sprayed and vacuum-sealed coatings. In the case of the vacuum-fused coating, the application of CP for 6 days under liquid impingement resulted in no measurable weight loss.

The weight loss data for solid-liquid impingement tests are presented in Table 3. It should first be noted that, even after a 1 h exposure to liquid-solid erosion conditions, the weight loss is greater than after 6 days in liquid erosion. Figure 3 shows the comparison in weight loss trends for the three coatings, and once again, it can be seen that the vacuum-sealed and as-sprayed coatings show a similar trend, and the vacuum-fused coating exhibits a much lower material loss rate. The TWL of the vacuum-fused coating was almost one-third in magnitude compared to the weight losses of as-sprayed and vacuum-sealed coatings under similar conditions after the 4 h tests. The application of CP again

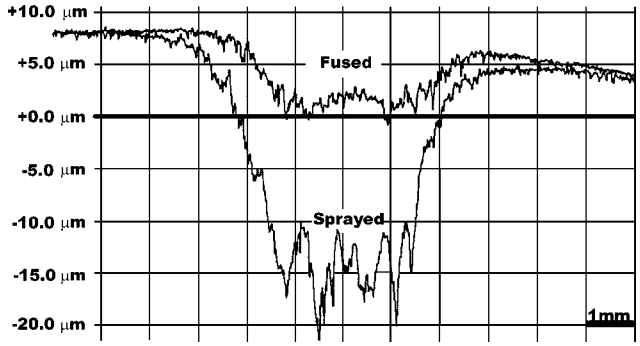

Fig. 4 Talysurf traces of central wear scars after 4 h solid-liquid impingement with CP

resulted in a substantial reduction of weight loss for all three coatings investigated; the effect being much more pronounced in the vacuum-fused coating, where a reduction of 75% after a 4 h exposure was achieved.

3.2 Surface Topography

The Talysurf traces (Fig. 4) of the wear scars under the impinging jet in solid-liquid conditions are in accordance with the higher-measured weight loss of the as-sprayed coating compared to that of the vacuum-fused coating. The as-sprayed coating exhibited a much deeper groove after the same exposure. Moreover, localized damage, in the form of several deep peaks and valleys inside the groove, was observed on the as-sprayed coating compared with a much smoother surface of the wear scar on the vacuum-fused coating sample but with maximum thickness loss out from the center of the scar. The maximum thickness loss of the sprayed coating ranged between 30 and 35 μm, where as that for the vacuum-fused coating ranged between 8 and 10 μm.

3.3 Anodic Polarization

The results of the anodic polarization sweeps of the coating with three different surface treatments in solid-free and solid-liquid impingement conditions are shown in Fig. 5. The polarization curves for all three coatings after 6 days solid-free impingement were similar and displayed what is regarded as classic passive behavior. This is represented by the very low currents measured over a wide range of potential from the free-corrosion potential, E_{corr}, to a value termed the breakdown potential, E_b, as shown in Fig. 5. The E_b values in Fig. 5 for all three coatings were similar, and all three coatings displayed sharp rises in the current densities after the breakdown potential.

In contrast, under solid-liquid impingement, the current density steadily increased, immediately after the potential was shifted to the positive potential direction from the E_{corr}. This is indicative of active corrosion occurring, which is an activation-controlled process and can be described by the well-known Tafel relationships. The corrosion current densities were determined by Tafel extrapolation[29] and are shown in Fig. 6. It can be seen that the corrosion current density of the fused coating was almost half of the values displayed by the as-sprayed and vacuum-sealed coatings.

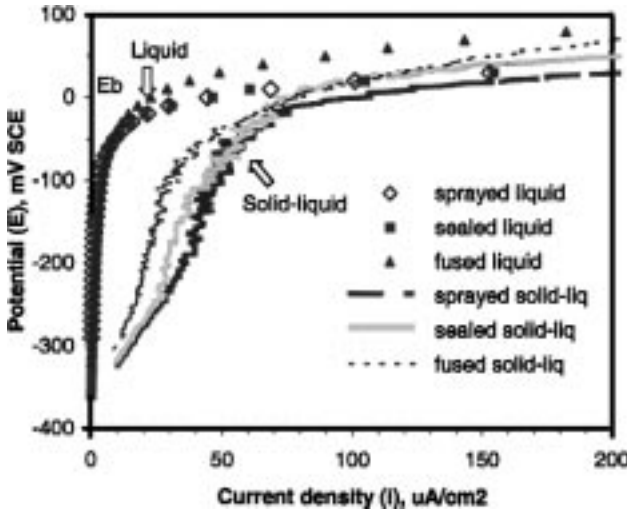

Fig. 5 Anodic polarization plots for coatings under liquid and liquid-solid erosion conditions at 17 m/s, 18 °C, 3.5% NaCl salt-water, and pH 8

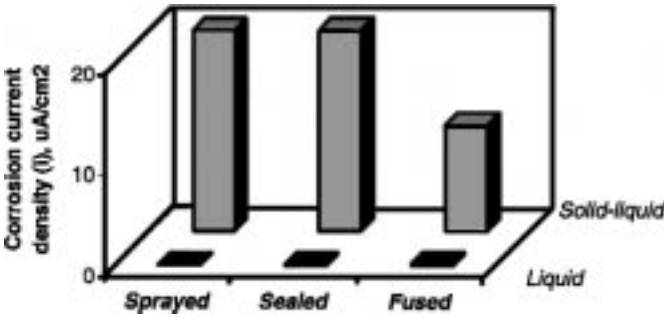

Fig. 6 Corrosion current densities for coatings under liquid and liquid-solid erosion conditions at 17 m/s and 18 °C

3.4 Microscopic Observations after Solid-Free Liquid Impingement

Corrosion products were easily visible on the as-sprayed and vacuum-sealed coatings, under both free-corrosion impingement and impingement with anodic polarization. On the macroscopic level, corrosion products in the form of comet-shaped streams were visible on the as-sprayed and vacuum-sealed coating just after 2 days of impingement, and significantly increased after the 6-day tests (Fig. 7(a)). These "comet" streams were principally seen in the area out from under the direct impingement zone (*i.e.*, out of the 1 mm diameter impingement zone). This feature has previously been observed on stainless steels and HVOF coatings after anodic polarization, as reported in previous communications.[25] In contrast, no such comets were observed on the vacuum-fused coating during the entire 6-day impingement tests (Fig. 7b).

Complex erosion-corrosion mechanisms were observed in the as-sprayed, vacuum-sealed, and vacuum-fused coatings. Damage on the as-sprayed and vacuum-sealed coatings was more at the macrolevel, comprising of preferential attack around the individual splat boundaries, resulting in bigger portions of material being removed as the individual particle splats dislodge (Fig. 8a). Furthermore, the comets comprised streams of corro-

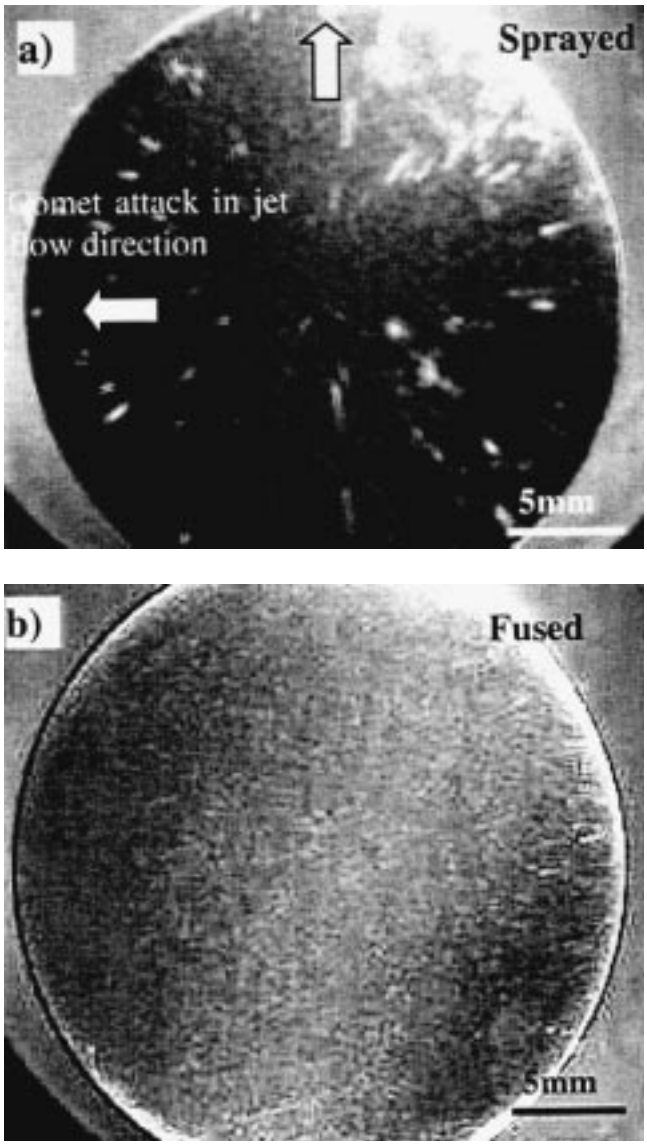

Fig. 7 After 6 days solid-free liquid impingement at 17 m/s, 3.5% NaCl, 18 °C: (**a**) comet pits on the surface of the as-sprayed coating and (**b**) surface of the vacuum-fused coating free from comet pits

sion product emanating from relatively deep holes, "macropits," at the comet head, excavating the subsequent coating layers (Fig. 8b). In addition, a smaller scale mechanism of attack was evident, associated with microgalvanic corrosion at the hard phases/matrix interfaces, resulting in their dislodgement forming "micropits" (Fig. 8c).

In the case of the vacuum-fused coating, the attack mechanisms were essentially at the microlevel, with "micropitting" occurring uniformly over the entire surface (Fig. 8d). The pits were very much smaller than the splat particles, which caused pit formation on the as-sprayed and vacuum-sealed coating.

The application of CP significantly reduced the extent of the damage on the as-sprayed and vacuum-sealed coatings during the 6 days of exposure (Fig. 9a and b). Moreover, under similar conditions of CP, no distinguishable attack was observed in case of the vacuum-fused coating.

3.5 Microscopic Observations after Solid-Liquid Impingement

Examination of specimens after solid-liquid impingement showed clear, central wear scars after just a 1 h test, demonstrating the much higher material loss with addition of solid particles. The low magnification photographs (Fig. 10a and b) show the higher material loss and rough surface on the as-sprayed coating under the impinging jet compared to the vacuum-fused coating and also show the much rougher wear-scar surface on the as-sprayed and vacuum-sealed coatings. The appearance of the vacuum-sealed coating was very similar to the as-sprayed type. The roughened surface seemed to result from a drilling action of the impinging sand-liquid slurry, which formed relatively large holes, "macropits" at the sites of which chunks of material were dislodged. The size of the holes was much larger than the average splat and was, therefore, not simply a result of splat dislodgement. A similar drilling effect has been previously observed during liquid-solid erosion of a similar Ni-Cr-Si-B-C HVOF-sprayed coating.[25] The enlargement of the pits was found to be associated with lateral crack propagation within the splat boundaries of as-sprayed and vacuum-sealed coatings, whereas the rupture mechanism in the case of the vacuum-fused coating was associated merely with ductile ploughing and some loss of hard-phase particles.

Material loss in coatings also occurred outside the central zone at low impact angles and formed craters and eventual material loss by removal of the raised lips from the crater on subsequent slurry impacts. Microscopic observations also revealed the loss of hard-phase particles being eroded away, together with the matrix being removed. Craters formed by the low-angle impact of the erodents on the as-sprayed and vacuum-sealed coatings (Fig. 11) were more severe than those on the vacuum-fused coating (Fig. 12). It should be noted that even under the liquid-solid erosion stream, corrosion at splat boundaries still occurred on both the as-sprayed and vacuum-sealed coatings (Fig. 13).

4. Discussion

The Ni-Cr-Mo-Si-B coating experiences low rates of material loss under solid-free liquid impingement in saline solution, but the rate of damage is increased by two orders of magnitude when the liquid contains 800 mg/L of suspended sand. Despite this "mechanically induced" acceleration of erosion-corrosion attack, the large reduction in material loss when corrosion was suppressed (Table 3) and the contribution to overall material loss by corrosion processes is still very significant in solid-liquid impingement.

In Part 1 of this work,[28] it was shown that the vacuum-fusion process on Ni-Cr-Mo-Si-B HVOF coating had very little effect on the resistance of the coating to corrosion initiation, but it changed the mechanisms of attack. This paper has demonstrated that vacuum-fusion offers clear benefits in improving erosion-corrosion resistance in aggressive solid-free and solid-containing liquid jets. This confirms that fusion of the coating to increase the proportion of hard-phase particles, coating density, and coating microhardness, and also to decrease porosity,[28] has a beneficial effect in terms of tribological performance alluded to in other work.[27]

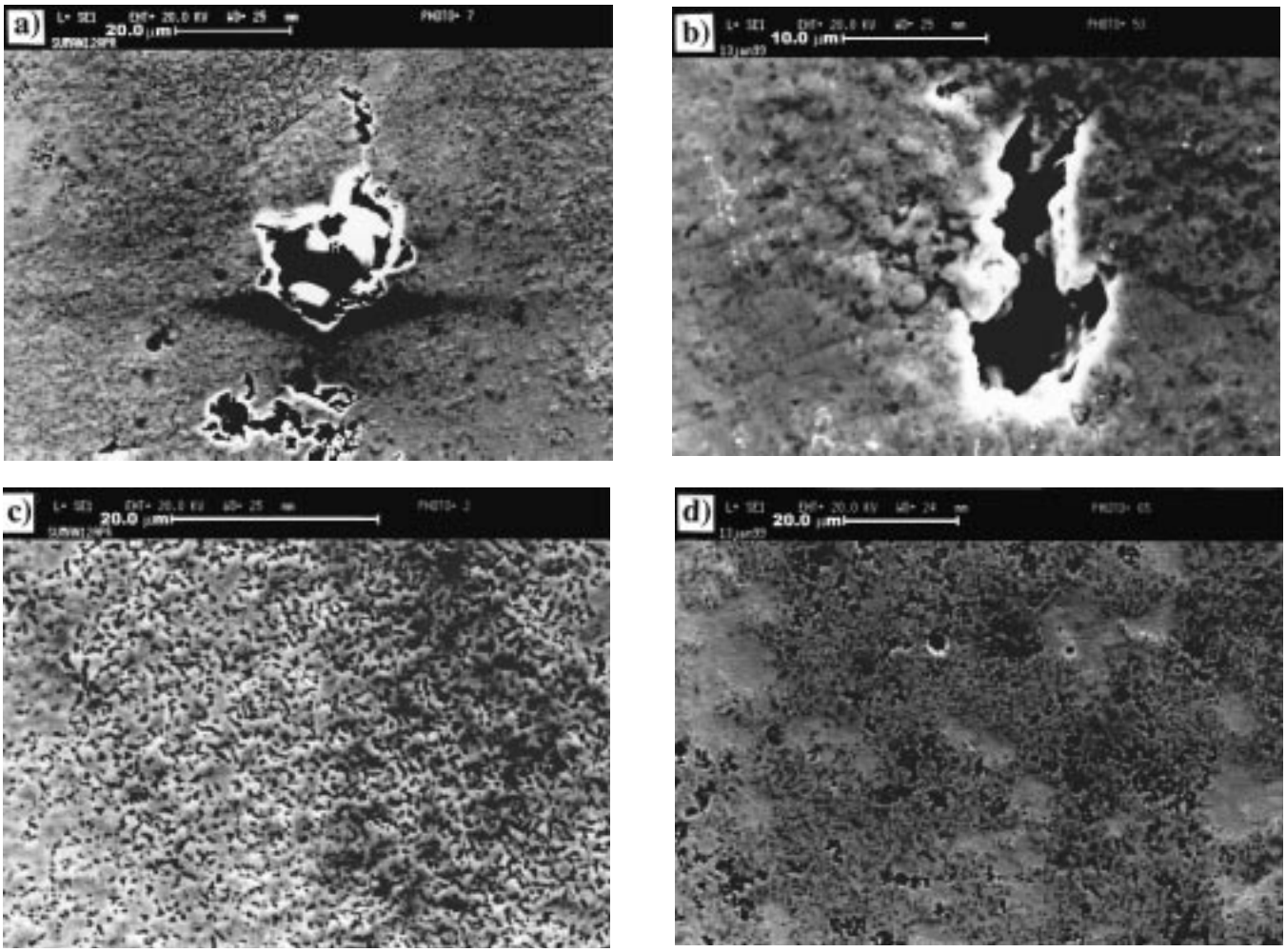

Fig. 8 (**a**) Individual splats removed (of as-sprayed coating) after 6 days of solid-free liquid impingement under 17 m/s jet velocity at 18 °C, (**b**) macropits formed at the head of comets on the as-sprayed coating after 6 days of liquid impingement, (**c**) micropitting formed by the removal of hard phase from the as-sprayed coating after 6 days of solid-free liquid impingement at 18 °C and 17 m/s, and (**d**) micropitting on the vacuum-fused coating caused by removal of hard phase after 6 days of solid-free liquid impingement at 18 °C and 17 m/s

4.1 Erosion-Corrosion Mechanism under Solid-Free Liquid Impingement Condition

The complex mechanism of material loss in as-sprayed and vacuum-sealed coatings was associated with preferential corrosion attack around splat boundaries, which resulted in removal of the loosened splats by liquid-jet impact under solid-free and/or liquid-solid impingement. Further attack on existing pits occurred due to the increased roughness of the surface at a microscale, and this caused formation of large and deep pits. This attack is a clear illustration of how the corrosion and mechanical erosion mechanisms can interact to cause severe degradation.

Corrosion of the binder matrix and the microgalvanic attack at the hard phase/matrix interface were also evident at several areas, as was reported as a key degradation mechanism in static conditions in Part 1.[28] Similar findings have also been reported on WC-CoCr coatings in Ref 22.

As discussed in Part 1, the corrosion mechanisms on the vacuum-fused coating were contrasting from the as-sprayed and vacuum-sealed coatings mainly due to the absence of splat boundaries in the former coating. The vacuum-fused coating exhibited material loss under erosion-corrosion conditions at the microlevel associated mainly with microgalvanic attack at the hard phase/matrix interface. Dissolution of the matrix also resulted in unsupported hard phases protruding out from the matrix, which further dislodged on subsequent liquid-jet impacts.

The application of CP significantly reduced the material loss in as-sprayed and vacuum-sealed coatings to almost half of that displayed in solid-free liquid impingement at the free-corrosion potential. The effect of CP was more pronounced in the case of the vacuum-fused coating, where no measurable material loss occurred under CP, signaling the important role of corrosion in determining the materials' overall erosion-corrosion resistance. The difference between the TWL under the free-corrosion condition and the material loss due to pure erosion during CP (E) is a measure of the contribution of the corrosion processes to the overall erosion-corrosion damage. These comprise a pure corrosion component (C), found by Tafel extrapolation from the anodic polarization, and a synergy component (S), *i.e.*,

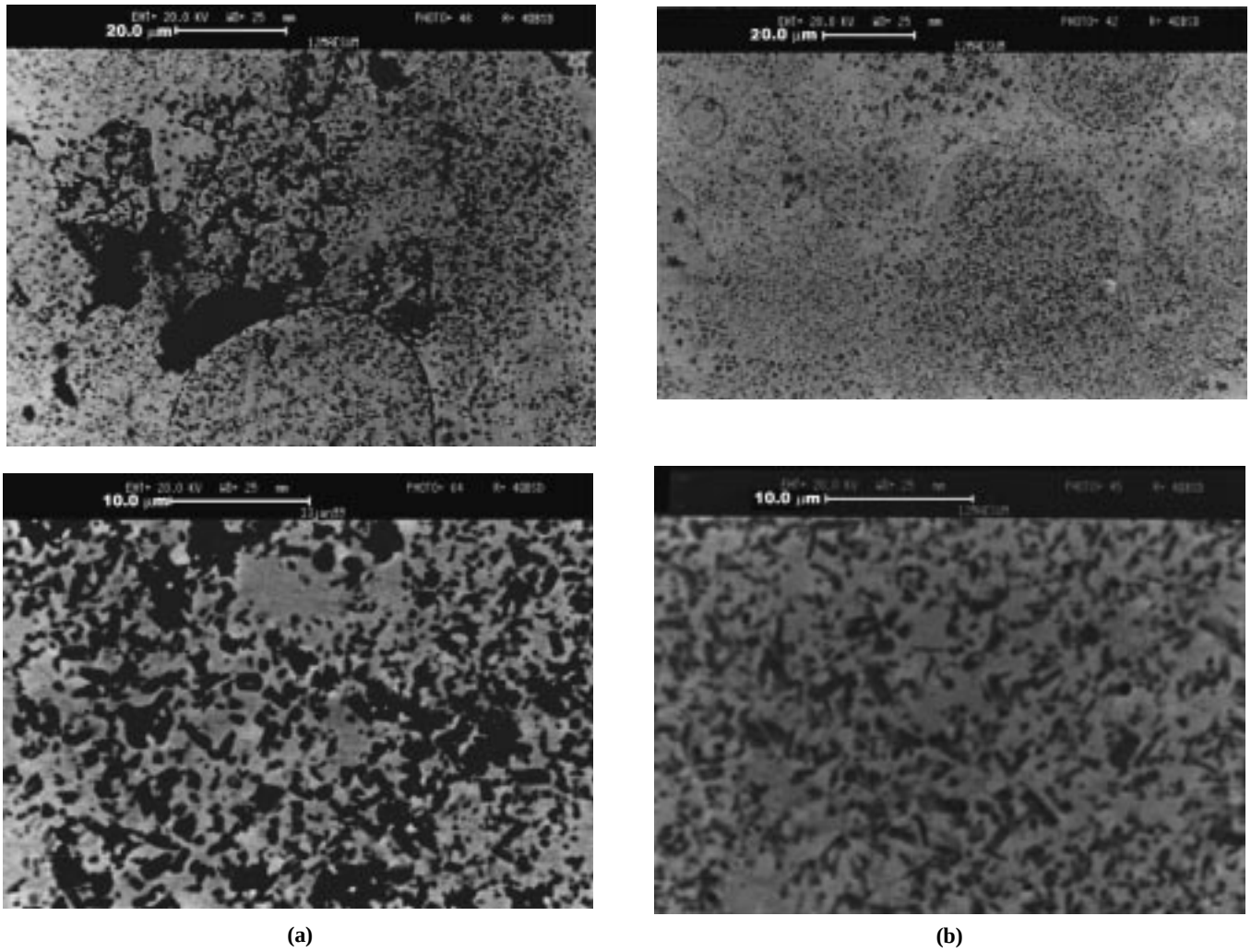

Fig. 9 (**a**) The SEM micrographs showing erosion-corrosion attack after 6 days of solid-free liquid impingement under 17 m/s jet velocity at 18 °C without CP on: as-sprayed coating (top) and vacuum-fused coating (bottom), and (**b**) SEM micrographs showing much reduced erosion-corrosion attack after 6 days of solid-free liquid impingement under 17 m/s jet velocity at 18 °C with applied CP at −0.8 V SCE on as-sprayed coating (top) and vacuum-fused coating with no sign of erosion-corrosion damage (bottom)

$$\text{TWL} = E + C + S \quad \text{(Eq 1)}$$

where *S* represents the effect of *corrosion* on increasing the *erosion* mass loss. Some other workers[6,30] similarly break down the TWL into components, which are summed, as shown in Eq 2:

$$\text{TWL} = E' + C' + dE_c + dC_e \quad \text{(Eq 2)}$$

where E' is the pure erosive component of the weight loss and is equivalent to E in Eq 1, C' is the corrosion rate of the material during flow without particles, dE_c is the change in erosion due to corrosion and is equivalent to S in Eq 1, and dC_e is the change in corrosion due to erosion. Hence, the term C in Eq 1, which is the electrochemical corrosion rate measured *in situ,* can be equated to $(C' + dC_e)$ in Eq 2.

In solid-free liquid conditions, the corrosion rates for all coatings were very small (about 0.001 mg/h) for the as-sprayed and vacuum-sealed coatings and about 0.002 mg/h for the vacuum-fused coating. For the vacuum-fused coating, the pure erosion component was zero under liquid impingement after 6 days, signaling that the TWL is governed by the synergy (Table 4). The increased resistance to pure mechanical material loss of the vacuum-fused coating compared with the nonfused coating could, in part, be a result of its increased hardness and density, as reported in Part 1.

4.2 Erosion-Corrosion Mechanism under Solid-Liquid Impingement Condition

Under solid-liquid impingement, as illustrated in Table 5, the corrosion rates were significantly increased compared with liquid erosion, but still, the pure corrosion component represented a relatively small proportion of the TWL on the three coatings. The value for *C* was 6% on the as-sprayed and vacuum-sealed coating and slightly greater, about 7%, on the fused coating. Notwithstanding the fact that the corrosion proportion was greater on the vacuum-fused coating, it should be noted here that the corrosion currents were lower (Fig. 6) on the vacuum-fused

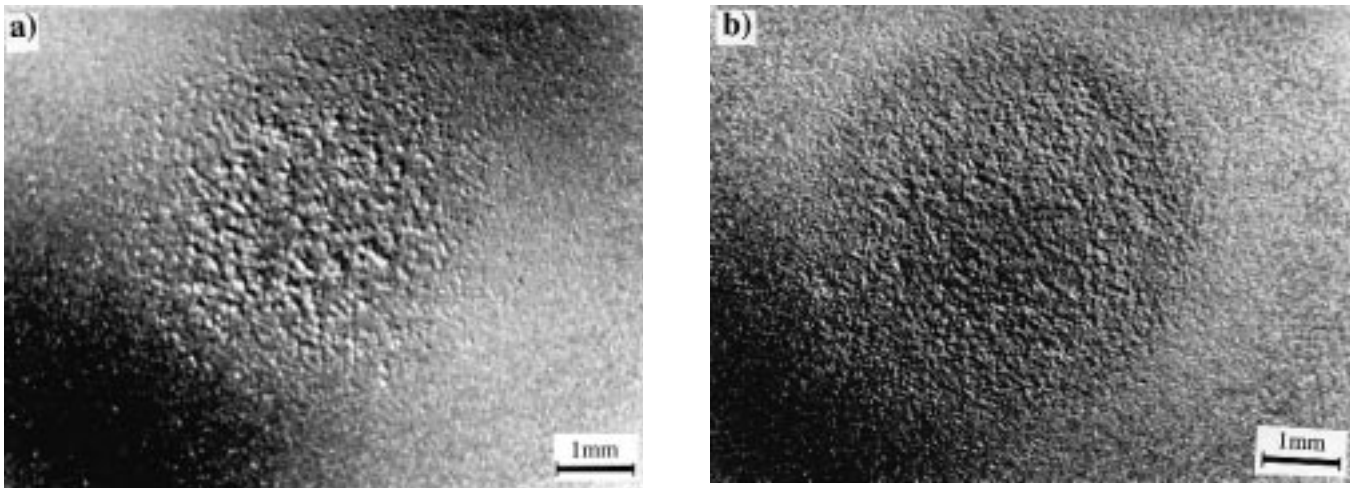

(a) **(b)**

Fig. 10 Wear scar after 1 h under liquid-solid conditions of (**a**) the as-sprayed coating and (**b**) the fused coating

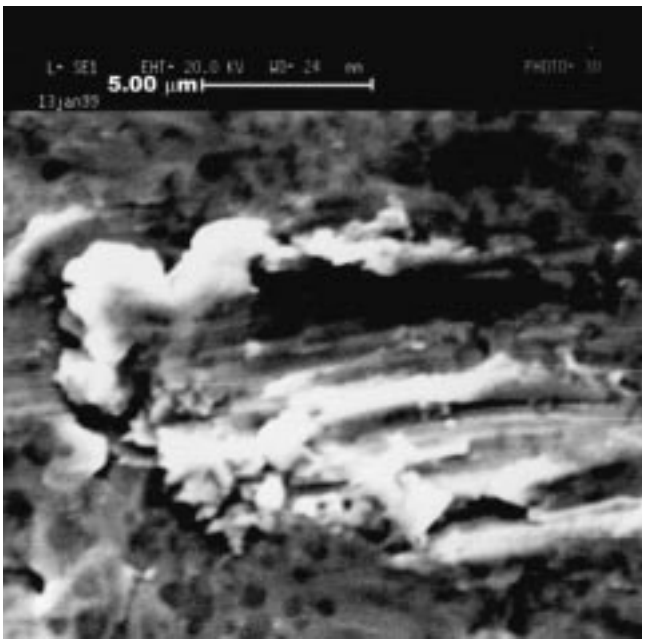

Fig. 11 Secondary SEM micrograph showing material removal mechanism at low angle during 1 h solid-liquid impingement on the as-sprayed coating

Table 4 Components of material loss *E*, *C*, and *S* after 6 days under solid-free liquid impingement

Material	TWL (mg/h)	*E* (%)	*C* (%)	*S* (%)
Sprayed	0.009	58	<0.1	42
Sealed	0.010	45	<0.1	55
Fused	0.004	0	<0.3	99.7

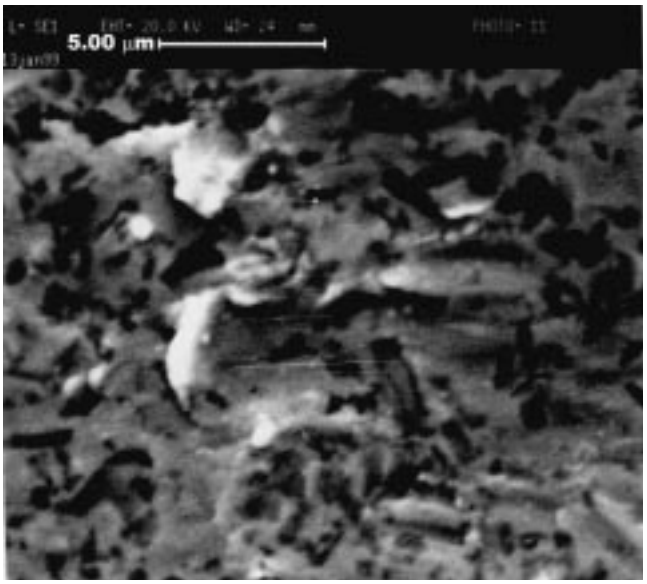

Fig. 12 Low-angle ploughing on the vacuum-fused coating after 1 h solid-liquid impingement

Table 5 Components of material loss *E*, *C*, and *S* after 1 h under 800 ppm solid-liquid impingement

Material	TWL (mg/h)	*E* (%)	*C* (%)	*S* (%)
Sprayed	1.5	63	6	31
Sealed	1.4	68	6	26
Fused	0.64	39	7	55

coating in contrast to the behavior in liquid erosion. This would appear to suggest that because the impact of the solids clearly removes less material on the vacuum-fused samples (as demonstrated from the lower weight loss under CP and the smaller craters formed at single impact sites), then, the corrosion current is lower as less material is "activated" through impact.

The pure erosion component of the as-sprayed and vacuum-sealed coatings are similar at 63 and 68%, whereas only 39% of the TWL on the vacuum-fused coating can be attributed to mechanical erosion. In terms of proportions, the synergistic com-

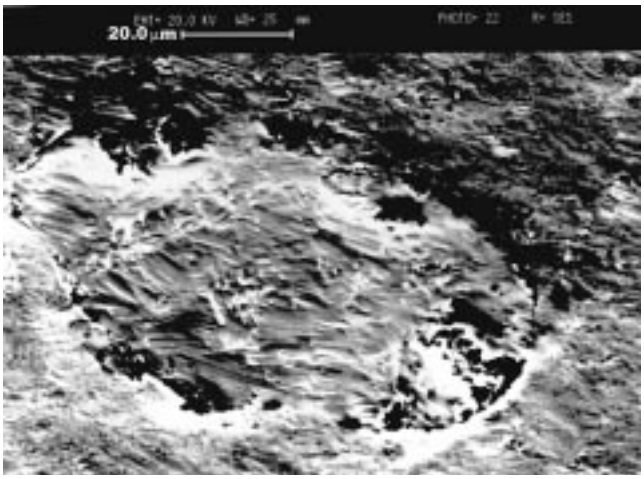

Fig. 13 Corrosion at the splat boundaries occurring under solid-liquid erosion conditions on the as-sprayed coating

ponent of weight loss dominates on the vacuum-fused coating, although in absolute terms, it is less than on the other two coatings. However, it is clear that corrosion affecting the mechanical erosion resistance of the coating is a main material-loss mechanism, and it would appear that this is dominated by corrosion of the matrix, which leads to easier mechanical removal of the hard phase. On the as-sprayed and vacuum-sealed coatings, this is further complicated by the corrosion initiation at splat boundaries, and there is potential for material to be lost in greater segments.

In this study, all tests have been conducted at a 90° angle of impingement, and analysis of the wear-scar profile has shown some interesting features, which may give insight into the effect of impingement angle on the different coatings. It can be seen from the profile on the vacuum-fused coating (Fig. 4) that there is a relatively high material removal at the region adjacent to the center of the wear scar, signifying low-angle attack, which is contrary to the more severe irregular-depth profile throughout the entire wear scar on the sprayed/sealed coating. This would appear to reflect on the fact that the vacuum-fused coating is behaving in a more ductile manner than the other coatings, and as such, the impingement is relatively greater at lower angles. This relationship was developed initially for dry erosion,[7] but several workers have observed the general trend in aqueous conditions.

5. Conclusions

- Under the erosion-corrosion conditions investigated, the material loss rates of the Ni-Cr-Mo-Si-B coatings were low during solid-free impingement but increased drastically in the presence of 800 mg/L of suspended sand particles.
- The work has demonstrated the complexity of erosion-corrosion mechanisms in the coating investigated and has identified significant corrosion and erosion interactions. Although, the direct corrosion contributions to erosion-corrosion damage are very small, substantial indirect corrosion effects (synergy) occur even under solid-liquid conditions.
- Postspray surface treatment by vacuum sealing reflected no effect on both solid-free and solid-liquid erosion-corrosion material losses from the coating. Post-treatment by vacuum-fusion offered substantial benefits in terms of erosion-corrosion resistance in both solid-free and solid-liquid impingement conditions. The effect of vacuum-fusion in consolidating the microstructure of the coating results in a more uniform pattern of erosion-corrosion damage.
- The application of cathodic protection generally produced significant benefits in reducing material loss but was more effective on the vacuum-fused coating than on the as-sprayed and vacuum-sealed coatings.
- The findings emphasize the potential benefits, in terms of erosion-corrosion resistance, of surface treatment of thermally sprayed coatings by the high-temperature fusion process.

Acknowledgment

This work was made possible by means of an ORS award and a Glasgow University Faculty of Engineering Research Scholarship made to S. Shrestha. The authors also acknowledge Professor J.W. Hancock, Head of the Mechanical Engineering Department, University of Glasgow, and Professor R.L. Reuben, Head of the Mechanical and Chemical Engineering Department, Heriot-Watt University, Edinburgh, for the provision of laboratory facilities.

References

1. K. Haugen, O. Kvernvold, A. Ronold, and R. Sandberg: *Wear,* 1995, vol. 186, pp. 179-88.
2. D.G. Elvery and K. Bremhorst: *Fluids Eng. Div. Conf.,* 1996, vol. 2, pp. 595-600.
3. A. Neville, T. Hodgkiess, and J.T. Dallas: *Wear,* 1995, vol. 186–187, pp. 497-507.
4. A. Neville: Ph.D. Thesis, University of Glasgow, Glasgow, United Kingdom, 1995.
5. B.W. Madsen: *Wear,* 1988, vol. 123, pp. 127-42.
6. S. Zhou, M.M. Stack, and R.C. Newman: *Corrosion,* 1996, vol. 52 (12), pp. 934-46.
7. I. Finnie: *Wear,* 1960, vol. 3, pp. 87-103.
8. I.M. Hutchings: *Tribology: Friction and Wear of Engineering Materials,* Edward Arnold, London, 1992.
9. A. Neville, T. Hodgkiess, and H. Xu: *Wear,* 1999, vol. 233–235, pp. 523-34.
10. D. Kumar and S.C. Modi: *Trans. Metal Finishers' Assoc. India,* 1995, vol. 4 (1), pp. 43-48.
11. D.W. Parket and G.L. Kutner: *Adv. Mater. Processes,* 1991, vol. 4, pp. 68-74.
12. R.B. Bhagat, J.C. Conway, M.F. Amateau, and R.A. Brezler: *Wear,* 1996, vol. 201 (1–2), pp. 233-243.
13. J. Wigren, L. Pejryd, and H. Karlsson: *Proc. 1st United Thermal Spray Conf.,* ASM International, Materials Park, OH, 1997, pp. 243-53.
14. K.T. Kembaiyan and K. Keshavan: *Wear,* 1995, vol. 186 (2), pp. 487-92.
15. B. Arsenault, J.G. Legoux, and H. Hawthorne: *Proc. 15th Int. Thermal Spray Conf.,* ASM International, Materials Park, OH, 1998, pp. 231-36.
16. M. Bjordal, E. Bardal, T. Rogne, and T.G. Eggen: *Wear,* 1995, vol. 186–187, pp. 508-14.
17. A. Karimi, C. Verden, J.L. Martin, and R.K. Schmid: *Wear,* 1995, vol. 186 (2), pp. 480-86.
18. T. Rogne, M. Bjordal, T. Solem, and E. Bardel: *Proc. 9th Nat. Thermal Spray Conf.,* C.C. Berndt, ed., ASM International, Materials Park, OH, 1996, pp. 207-15.
19. T. Rogne, T. Solem, and J. Berget: *Proc. 10th Nat. Thermal Spray Conf.,*

C.C. Berndt, ed.; ASM International, Materials Park, OH, 1997, pp. 113-19.
20. S. Shrestha, T. Hodgkiess, and A. Neville: *12th Int. Conf. Wear Materials*, D.A. Rigney and R.G. Bayer, eds., Elsevier, Amsterdam, 1999, poster paper.
21. A. Neville and T. Hodgkiess: *Surface Eng.*, 1996, vol. 12 (4), pp. 303-12.
22. A. Neville and T. Hodgkiess: *Proc. 10th Nat. Thermal Spray Conf.*, ASM International, Materials Park, OH, 1997, pp. 161-67.
23. T. Hodgkiess and A. Neville: *Proc. 15th Int. Thermal Spray Conf.*, ASM International, Materials Park, OH, 1998, pp. 63-68.
24. T. Hodgkiess and A. Neville: *Proc. 1st United Thermal Spray Conf.*, ASM International, Materials Park, OH, 1997, pp. 167-74.
25. T. Hodgkiess, A. Neville, and S. Shrestha: *Wear*, 1999, vol. 233–235, pp. 623-34.
26. L. Pawlowski: *The Science and Engineering of Thermal Sprayed Coatings*, John Wiley & Sons, New York, NY, 1994.
27. N.H. Sutherland and D. Wang: in *Surfacing Engineering*, P.K. Datta and J.S. Gray, eds., The Royal Society of Chemistry, Cambridge, United Kingdom, 1993, vol. 3, pp. 26-36.
28. S. Shrestha, A. Neville, and T. Hodgkiess: *J. Thermal Spray Technol.*, 2001, vol. 10(3), pp. 470-79.
29. S. Shrestha: Ph.D. Thesis, University of Glasgow, Glasgow, United Kingdom, 2000.
30. M. Bjordal: Ph.D. Thesis, University of Trondheim, Trondheim, Norway, 1995.